Designing a radiative antidote to CO_2

Jacob T. Seeley[1], **Nicholas J. Lutsko**[2], **David W. Keith**[3]

[1]Harvard University Center for the Environment

[2]Scripps Institution of Oceanography

[3]John A. Paulson School of Engineering and Applied Sciences (SEAS), Harvard Kennedy School, Harvard University

Key Points:

- Spectrally-flat solar geoengineering reduces CO_2-induced change in mean rainfall disproportionately more than mean temperature.
- A spectrally-tuned sunshade restores mean temperature and rainfall simultaneously in an idealized model.
- Emerging technologies could preferentially scatter sunlight in the near-infrared, providing a spectral sunshade.

Corresponding author: Jacob T. Seeley, jacob.t.seeley@gmail.com

This article has been accepted for publication and undergone full peer review but has not been through the copyediting, typesetting, pagination and proofreading process, which may lead to differences between this version and the Version of Record. Please cite this article as doi: 10.1029/2020GL090876.

Abstract

Solar Radiation Modification (SRM) reduces the CO_2-induced change to the mean global hydrological cycle disproportionately more than it reduces the CO_2-induced increase in mean surface temperature. Thus if SRM were used to offset all CO_2-induced mean warming, global-mean precipitation would be less than in an unperturbed climate. Here we show that the mismatch between the mean hydrological effects of CO_2 and SRM may partly be alleviated by spectrally tuning the SRM intervention (reducing insolation at some wavelengths more than others). By concentrating solar dimming at near-infrared wavelengths, where H_2O has strong absorption bands, the direct effect of CO_2 on the tropospheric energy budget can be offset, which minimizes perturbations to the mean hydrological cycle. Idealized cloud-resolving simulations of radiative-convective equilibrium confirm that spectrally-tuned SRM can simultaneously maintain mean surface temperature and precipitation at their unperturbed values even as large quantities of CO_2 are added to the atmosphere.

Plain Language Summary

It may be possible to partly counteract CO_2-driven climate change by solar radiation modification (SRM) that intentionally reduces the amount of sunlight absorbed by the Earth. But different wavelengths of the solar spectrum are absorbed at different altitudes within the surface-atmosphere system, so different climatic effects are to be expected depending on which wavelengths of sunlight are affected by an SRM intervention. Here we show that if the goal is to minimize perturbations to the mean hydrological cycle, the ideal spectrally-tuned SRM intervention may need to focus on near-infrared wavelengths. This study clarifies the basic physics underlying the effects of SRM on atmospheric energetics and the mean hydrological cycle.

1 Introduction

Solar Radiation Modification (SRM) proposals aim to counteract CO_2-driven climate change by reducing the amount of sunlight absorbed by the Earth (D. Keith, 2013). Although significant scientific, practical, and ethical questions remain (e.g., P. J. Irvine et al., 2016; Preston, 2013), a growing body of evidence supports the notion that SRM could reduce many climatic changes that normally accompany a rise in CO_2 (e.g., Govindasamy & Caldeira, 2000; P. Irvine et al., 2019). Yet the interventions proposed for SRM

do not exactly counteract the radiative impacts of CO_2 forcing, so SRM would not exactly offset CO_2-driven climate change. For example, a robust feature identified in simulations of geo-engineered climates is a weakened global hydrological cycle (Kravitz, Caldeira, et al., 2013). That is, simulations of climates with high CO_2 and a dimmer sun have lower mean precipitation and evaporation than do unperturbed climates with the same global-mean temperature but lower CO_2 and a brighter sun (e.g., Bala et al., 2008; Tilmes et al., 2013; Smyth et al., 2017).

The cause of the damped hydrological cycle in geo-engineered climates is well understood in terms of atmospheric energetics (e.g., Bala et al., 2008; Kravitz, Rasch, et al., 2013; Kleidon et al., 2015). All else being equal, adding CO_2 to the atmosphere reduces the longwave (LW) cooling of the troposphere, and since the radiative cooling of the troposphere is balanced primarily by latent heat released in precipitating clouds, a reduction in radiative cooling leads to a reduction in precipitation (e.g. Allen & Ingram, 2002; Andrews et al., 2010). This is one of the "direct effects" of CO_2, so-called because they are not mediated by changes in surface temperature (Dinh & Fueglistaler, 2017; Romps, 2020). Since the direct effect of CO_2 on tropospheric radiative cooling has remained largely uncompensated in the SRM interventions that have been modeled so far, reductions in mean precipitation have been identified as a robust feature of geo-engineered climates (Kravitz, Caldeira, et al., 2013).

But, is this reduction in mean precipitation really an inevitable outcome of SRM interventions? The purpose of this study is to explore, theoretically and in the context of an idealized model, the possibility of a more complete radiative antidote to CO_2 forcing — an antidote that simultaneously maintains mean temperature and precipitation at their unperturbed values even as CO_2 is added to the atmosphere. Our approach exploits the fact that the shortwave (SW) opacity of the troposphere is not evenly distributed across the solar spectrum, which means that different wavelengths of sunlight deposit their energy within different layers of the coupled surface-troposphere system (Haigh et al., 2010). This allows a spectrally-tuned SRM intervention (i.e., a wavelength-dependent reduction in insolation) to restore energy balance at the tropopause and at the surface simultaneously. As a result, spectrally-selective SRM could be less disruptive to the mean hydrological cycle than spectrally-uniform SRM, which is the style of intervention that has been modelled by the majority of previous studies (e.g., the "G1" experiment from the recent GeoMIP project; Kravitz et al., 2011).

It is not currently known to what extent changes to regional precipitation in geoengineered climates result from the physics we explore here — that is, from the mismatch between the effects of CO_2 and SRM on the tropospheric energy budget. Other factors, such as spatial or seasonal mismatches between CO_2 and SRM forcing (e.g., Lutsko et al., 2020), or stratospheric heating due to aerosol injection (Simpson et al., 2019), may dominate over the mean-energetics perspective that is the focus of our study. Future work investigating the effects of spectrally-tuned SRM interventions with a comprehensive global climate model will help to answer this important question. While our focus is on an idealized model, we review progress toward achieving spectrally-selective SRM in the real world, and note that the methods and physical insight gained from our approach are relevant to all SRM because no SRM intervention would be exactly spectrally uniform.

2 Theory

The use of SRM interventions to counteract CO_2 forcing is motivated by the standard forcing-feedback framework for temperature change (e.g., S. C. Sherwood et al., 2015), which states that the equilibrium change in surface temperature, ΔT_s, produced by an external perturbation is proportional to the radiative forcing at the tropopause produced by that perturbation, F_t (W/m^2):

$$\Delta T_\mathrm{s} = \alpha_T F_\mathrm{t}, \tag{1}$$

where the constant of proportionality α_T (K/W/m^2) is known as the "climate sensitivity" parameter. In this context, radiative forcing refers to the change in net radiative flux produced by the perturbation itself (i.e., before any adjustments in surface temperature). Motivated by equation (1), the SRM interventions previously modeled in the literature have aimed to lessen CO_2-induced warming by offsetting the (positive) CO_2 radiative forcing at the tropopause with a countervailing (negative) radiative forcing at the tropopause from SRM.

While the energy budget at the tropopause controls changes in surface temperature, it alone does not constrain the precipitation rate because changes in precipitation ΔP (kg/m^2/s) are driven by changes in *tropospheric* radiative cooling, ΔQ (W/m^2):

$$\Delta P = -\alpha_P \Delta Q, \tag{2}$$

where α_P (kg/J) is a "hydrological sensitivity" parameter[1] (e.g., O'Gorman et al., 2011; Pendergrass & Hartmann, 2014), and where negative values of Q indicate the typical situation of net tropospheric radiative cooling. Since tropospheric radiative cooling depends on surface temperature as well as external perturbations such as increased CO_2 or changes in insolation, it is useful to separate ΔQ into the component produced by external perturbations and the component that depends explicitly on ΔT_s (Lambert & Faull, 2007):

$$\Delta Q = F_\mathrm{a} + \frac{\partial Q}{\partial T_\mathrm{s}} \Delta T_\mathrm{s}. \tag{3}$$

Here the external perturbation component F_a can be regarded as a radiative forcing of the troposphere, which is simply the difference between the radiative forcing of the external perturbation evaluated at the tropopause and at the surface:

$$F_\mathrm{a} = F_\mathrm{t} - F_\mathrm{s}. \tag{4}$$

From equations (1–4), we can deduce that a "radiative antidote" to CO_2 that maintains $\Delta T_\mathrm{s} = \Delta P \simeq 0$ must offset the CO_2 radiative forcing at the tropopause and at the surface simultaneously.

Is such a radiative antidote to CO_2 possible? The left column of Figure 1 shows a schematic depiction of the radiative forcings produced by increased CO_2: a positive forcing at the tropopause $F_\mathrm{t}^{\mathrm{CO_2}}$, and a smaller positive forcing at the surface $F_\mathrm{s}^{\mathrm{CO_2}}$. For a given perturbation x, it is convenient to define a measure of how suppressed the associated radiative forcing is at the surface compared to at the tropopause:

$$\epsilon_x \equiv F_\mathrm{s}^x / F_\mathrm{t}^x. \tag{5}$$

For example, for a CO_2 perturbation, the global-mean surface forcing is about half as large as the global-mean tropopause forcing (i.e., $\epsilon_{\mathrm{CO_2}} \simeq 0.5$; Huang et al., 2017).

How do the surface and tropopause forcings compare for SRM interventions? The answer depends on 1) the shortwave opacity of the troposphere, and 2) the spectral signature of the SRM intervention. The most commonly-studied SRM intervention is the idealized "sunshade" experiment ("G1") from the GeoMIP protocol (Kravitz et al., 2011). This experiment calls for a simple reduction in the solar constant, which is implemented in numerical models as a spectrally-uniform fractional reduction in downwelling shortwave at the top-of-atmosphere (TOA). For this style of spectrally-flat SRM, ϵ_{SRM} de-

[1] Note that others have defined the hydrological sensitivity as $\Delta P / \Delta T_\mathrm{s}$ (e.g., Kleidon et al., 2015).

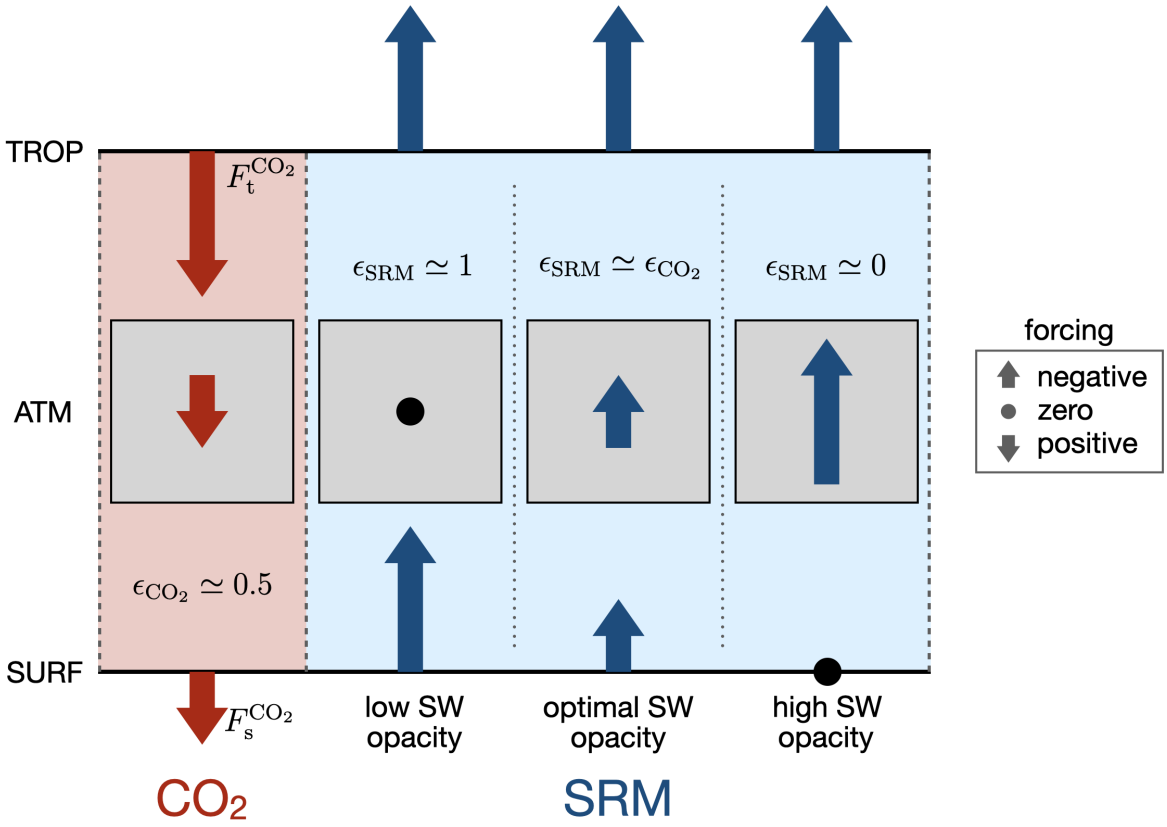

Figure 1. A schematic depiction of the radiative forcings at the tropopause (TROP), surface (SURF), and within the troposphere (ATM) produced by increasing CO_2 (leftmost column), or by idealized "sunshade" SRM interventions (three columns at right) in the style of the G1 experiment from GeoMIP (Kravitz et al., 2011). The SRM case is split into three sub-cases with bulk tropospheric shortwave opacities increasing from left to right. For a given perturbation x, ϵ_x is the ratio between the associated radiative forcing at the surface and at the tropopause: $\epsilon_x \equiv F_s^x / F_t^x$. Standard G1-style SRM falls toward the low end (left column) of the SW opacity scale.

pends on the bulk shortwave opacity of the troposphere: for a troposphere that is completely (i.e., at all wavelengths) transparent to sunlight, $F_t^{SRM} = F_s^{SRM}$ and $\epsilon_{SRM} = 1$, whereas for a troposphere that is completely opaque to sunlight, F_t^{SRM} is finite while $F_s^{SRM} = 0$, and so $\epsilon_{SRM} = 0$ (Figure 1, columns 2 and 4).

The above considerations allow us to understand what happens to the hydrological cycle when a CO_2 perturbation is combined with a sunshade-type SRM intervention. Combining equations (1–5), and setting $F_t^{CO_2} = -F_t^{SRM}$ as specified by the G1

GeoMIP protocol, we obtain the following expression for the change in precipitation:

$$\Delta P = \alpha_P F_{\mathrm{t}}^{\mathrm{CO_2}} \left(\epsilon_{\mathrm{CO_2}} - \epsilon_{\mathrm{SRM}}\right). \tag{6}$$

Hence the only circumstance in which spectrally-flat SRM can counteract CO_2 forcing at the tropopause and at the surface simultaneously is if the troposphere happens to have the correct intermediate bulk shortwave opacity so that $\epsilon_{\mathrm{SRM}} = \epsilon_{\mathrm{CO_2}}$. Otherwise, if a spectrally-flat SRM intervention is scaled such that $F_{\mathrm{t}}^{\mathrm{SRM}}$ completely counteracts $F_{\mathrm{t}}^{\mathrm{CO_2}}$, there will be a residual radiative forcing of the troposphere. This residual forcing will drive a change in convective enthalpy fluxes from the surface (e.g., Dinh & Fueglistaler, 2017), and perturb the hydrological cycle according to equations (2–3), as has been observed in the GeoMIP G1 experiment (Kravitz, Caldeira, et al., 2013; Tilmes et al., 2013). From the fact that the G1 experiment has yielded *reduced* mean precipitation (i.e., $\Delta Q > 0$), we can deduce that the bulk shortwave opacity of Earth's contemporary troposphere is too low (i.e., $\epsilon_{\mathrm{SRM}} > \epsilon_{\mathrm{CO_2}}$) for a spectrally-flat solar dimming to offset the direct effect of CO_2 on tropospheric radiative cooling. By constrast, a spectrally-tuned SRM intervention could, in principle, concentrate the solar dimming in a portion of the solar spectrum with above-average tropospheric shortwave opacity, thereby allowing $\epsilon_{\mathrm{SRM}} \simeq \epsilon_{\mathrm{CO_2}}$ by construction. This is the basic insight underlying our suggestion that spectrally-tuned solar dimming could be a more complete radiative antidote to CO_2 forcing.

To quantitatively explore the potential of spectrally-tuned solar dimming, let us split the downwelling shortwave radiation at the tropopause, $S_{\mathrm{t}}^{\downarrow}$, into N bands indexed by i, each with incoming power S_i ($\mathrm{W/m^2}$):

$$S_{\mathrm{t}}^{\downarrow} = \sum_{i=1}^{N} S_i \tag{7}$$

In each of these bands, we denote the tropospheric transmissivity to vertically-propagating radiation as $\mathcal{T}_i = e^{-\tau_i}$, where τ_i is the total tropospheric column SW optical depth[2] in band i (assumed to be uniform within the band). If S_i is reduced by some fraction, the ratio of the associated forcings at the surface and tropopause is found, via Beer's law, to be

$$\epsilon_i = \frac{\mathcal{T}_i^{1/\overline{\mu}}(1-a_i)}{1-a_i\mathcal{T}_i^{1/\overline{\mu}+D}}, \tag{8}$$

[2] For simplicity, here we assume SW attenuation is due only to molecular absorption, which is true for clear skies at wavelengths where Rayleigh scattering is negligible (e.g., the near-infrared).

where $\overline{\mu}$ is the effective cosine of the solar zenith angle, $D = 1.5$ is a two-stream hemispheric diffusivity factor (Clough et al., 1992), and where we have assumed a Lambertian surface with a band-specific SW albedo a_i. The optimal shortwave optical depth τ^* for offsetting CO_2 forcing is found by setting ϵ_i as given by equation (8) equal to ϵ_{CO_2}. To get a rough sense of the numbers, we can take $\epsilon_{CO_2} = 0.5$ and $a_i = 0$, yielding

$$\tau^* = \overline{\mu} \ln(2) \simeq 0.46, \tag{9}$$

where we have assumed $\overline{\mu} = 2/3$ (as is appropriate for the global mean; Cronin, 2014). For $a_i \neq 0$, τ^* is easily obtained via a rootsolver.

Now suppose we reduce the downwelling SW at the tropopause by band-specific fractional amounts γ_i, for $0 \leq \gamma_i \leq 1$ ($\gamma_i = 0$ corresponds to no reduction at the tropopause, whereas $\gamma_i = 1$ corresponds to complete blocking). The challenge of spectrally-tuned solar dimming amounts to finding a set of γ_i (i.e., a spectral filter) that simultaneously offsets $F_{\mathrm{t}}^{\mathrm{CO_2}}$ and $F_{\mathrm{s}}^{\mathrm{CO_2}}$, which is equivalent to simultaneously solving the following two equations:

$$F_{\mathrm{t}}^{\mathrm{CO_2}} = \sum_{i=1}^{N} \gamma_i S_i (1 - a_i \mathcal{T}_i^{1/\overline{\mu}+D}), \tag{10}$$

$$F_{\mathrm{s}}^{\mathrm{CO_2}} = \sum_{i=1}^{N} \gamma_i S_i \mathcal{T}_i^{1/\overline{\mu}} (1 - a_i). \tag{11}$$

To that end, it is instructive to consider a few limiting cases:

1. Filtering a band that passes through the atmosphere unabsorbed ($\mathcal{T}_i = 1$) perturbs the tropopause and surface energy budgets by the same amount, $\gamma_i S_i (1 - a)$.
2. Filtering a band that is completely absorbed in the troposphere ($\mathcal{T}_i = 0$) perturbs the tropopause energy budget by $\gamma_i S_i$, while leaving the surface energy budget unaffected.
3. Filtering a band for which $\mathcal{T}_i^{1/\overline{\mu}}(1-a)/\left[1 - a\mathcal{T}_i^{1/\overline{\mu}+D}\right] = \epsilon_{CO_2}$ offsets the same *fraction* of CO_2 forcing at the tropopause and at the surface.

These principles suggest that there are many equally valid algorithms that could be used to design a spectral SRM filter. For simplicity, in this work we will simply find a contiguous band of wavenumbers that happens to have the correct distribution of optical depths to simultaneously solve (10–11).

3 Experimental methods

Our understanding of the effect of SRM on global-mean precipitation is based on a radiative-convective equilibrium (RCE) perspective on the tropospheric energy budget (Bala et al., 2008; Kravitz, Rasch, et al., 2013; Kleidon et al., 2015). The state of RCE is the simplest system that faithfully captures the vertically-resolved energy budget of Earth's troposphere — that is, the balance between radiative cooling and convective heating. Therefore, the RCE framework is a natural testbed for a proof-of-principal demonstration of spectral SRM. We conducted RCE simulations with the cloud-resolving model DAM (Romps, 2008), which has been used extensively to study tropical convection in Earth's atmosphere (e.g., Romps & Kuang, 2010; Romps, 2011, 2014; Seeley & Romps, 2015, 2016; Seeley, Jeevanjee, Langhans, & Romps, 2019; Seeley, Jeevanjee, & Romps, 2019). The default radiation scheme in DAM is RRTM (Clough et al., 2005; Iacono et al., 2008), a correlated-k code, but for the purpose of this study we have coupled DAM to a clear-sky radiation scheme based on the PCM-LBL code (Wordsworth et al., 2017). This radiation scheme simply integrates the radiative transfer equation on a user-supplied spectral grid using standard molecular opacity data from the HITRAN database (Gordon et al., 2017), a "brute-force" (i.e., wavenumber-by-wavenumber) approach to radiation that greatly facilitates the investigation of spectrally-tuned solar dimming without meaningful reductions in accuracy. We have benchmarked our radiation scheme against RRTM and a line-by-line radiation code for an appropriate range of clear-sky conditions and find very good agreement (Figures S2-3). In addition, whereas DAM typically uses the Lin-Lord-Krueger bulk microphysics scheme (Lin et al., 1983; Lord et al., 1984; Krueger et al., 1995), for this study we use the simplified cloud microphysics parameterization described in Seeley, Jeevanjee, & Romps (2019). Since we adopt a clear-sky perspective here, our results are not sensitive to the microphysics scheme, and we believe that the simplified treatment of microphysics is appropriate for the present study, which is intended simply as a proof-of-principle. Our simulations were conducted with a horizontal resolution of $\Delta x = 2$ km on a square domain with a side length of approximately 100 km and doubly-periodic horizontal boundary conditions. For further details regarding the numerical modelling configuration, see the Supporting Information.

We first ran a control experiment (referred to as "CTRL") with a total solar irradiance (TSI) of 510.375 W/m^2 and a fixed cosine of the solar zenith angle of $\overline{\mu} = 2/3$ (Cronin, 2014), yielding a downwelling shortwave flux at the TOA of 340.25 W/m^2; this

value matches the planetary-mean insolation $\mathcal{S}_0/4$, where $\mathcal{S}_0 = 1361$ W/m^2 is the solar constant. The CTRL simulation was specified to have a preindustrial CO_2 concentration of 280 ppm and no ozone. CTRL was initialized from a similar RCE simulation over a fixed sea surface temperature and run for 1 year over a slab-ocean surface with a wavelength-independent albedo of 0.285, infinite horizontal conductivity (i.e., a uniform temperature), and heat capacity equivalent to a layer of liquid water of depth 20 cm. Results for CTRL were averaged over the final 200 days of model time. The equilibrated state of CTRL has a slab-ocean temperature of 288.64 K and mean precipitation rate of 3.17 mm/day. We then branched three experiments from the equilibrated state of CTRL: an abrupt quadrupling of CO_2 (referred to as "4×CO_2"), and two experiments for which the CO_2 quadrupling was accompanied by the application of some type of SRM. These branched simulations were run for an additional 3 years of model time, with results averaged over the final 100 days.

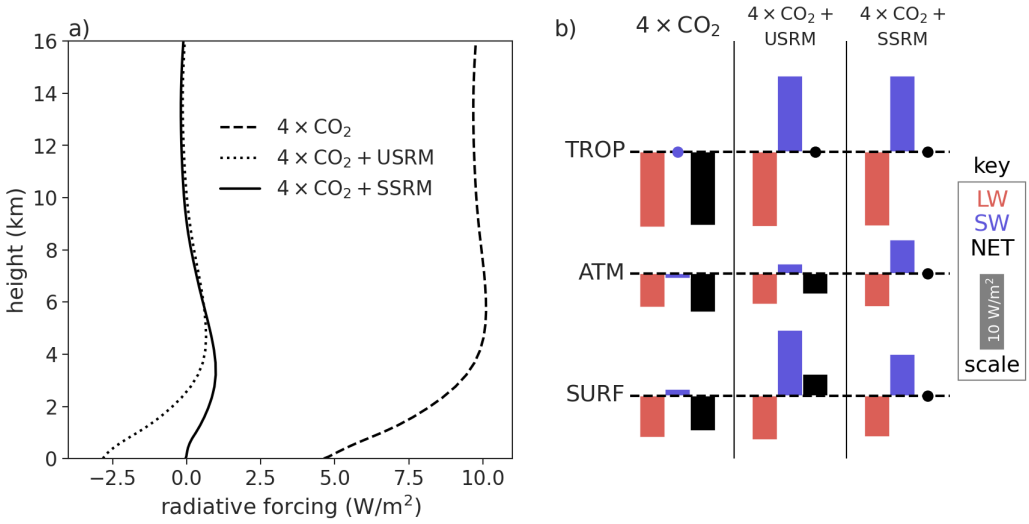

Figure 2. (a) Vertically-resolved radiative forcings, diagnosed as differences in net radiative fluxes. The forcings are shown for the three branched simulations with quadrupled CO_2, two of which also include an SRM interventions (USRM or SSRM) as described in the main text. (b) Radiative forcings evaluated at the tropopause (top row, TROP; $z \simeq 15$ km), surface (bottom row, SURF), and within the troposphere (middle row, ATM = TROP - SURF). For each simulation and level, the longwave (LW), shortwave (SW), and net (LW+SW) forcings are color-coded. By convention, positive forcings are depicted as downward-pointing bars, with the scale indicated by the gray 10 W/m^2 bar shown in the key; forcings with magnitude less than 0.2 W/m^2 are depicted as filled circles.

The SRM interventions were designed according to the principles discussed in section 2. We first calculated the instantaneous radiative forcing from a quadrupling of CO_2 by double-calling the radiative transfer scheme at every radiative time step of the CTRL simulation (once with 280 ppm CO_2 and once with 1120 ppm CO_2), and taking the difference between the net radiative fluxes. We evaluated these forcings at the tropopause and at the surface; the tropopause was identified as the level at the top of the troposphere where the time-averaged cloud fraction in CTRL falls below 1% (an altitude of approximately 15 km). For the CO_2 quadrupling, the instantaneous radiative forcing at the tropopause was found to be $F_\mathrm{t} = 9.71$ W/m^2, while the forcing at the surface was $F_\mathrm{s} = 4.63$ W/m^2 (Fig. 2; see also Table 1). Note that this implies $\epsilon_{\mathrm{CO}_2} \simeq 0.5$ in our CTRL experiment, close to the global-mean value reported in the literature (Huang et al., 2017). Strictly speaking, the forcing F_t that enters into the forcing-feedback framework of equation (1) should be the so-called *adjusted* forcing, which is the radiative flux imbalance at the tropopause after stratospheric temperatures adjust to return the stratosphere to radiative equilibrium (e.g., Smith et al., 2018). For simplicity, here we use the instantaneous forcing in place of the adjusted forcing, which was not found to be a large source of error.

In accordance with the GeoMIP G1 experiment (Kravitz et al., 2011), our first SRM intervention was designed to completely offset the CO_2 radiative forcing at the tropopause by reducing the solar constant. Since this amounts to a spectrally-uniform reduction in TOA downwelling shortwave, we will refer to this intervention as USRM (with the "U" indicating that this intervention is spectrally-uniform). The net shortwave flux at the tropopause in CTRL is $S_\mathrm{t} = 259.0$ W/m^2, so we reduced the TSI by the factor $F_\mathrm{t}/S_\mathrm{t} = 3.75\%$ (from 510.375 W/m^2 to 491.23 W/m^2). To assess the efficacy of the intervention, we averaged the radiative fluxes over the first week of the branched simulation, and calculated radiative forcings as differences between these radiative fluxes and the mean radiative fluxes from CTRL. As can be seen in the middle column of Figure 2b ($4\times CO_2$+USRM), this spectrally-uniform SRM intervention restores the energy budget at the tropopause (i.e., there is a negligible difference in net radiative flux at the tropopause between CTRL and $4\times CO_2$+USRM), due to a cancellation between the positive LW forcing from the CO_2 perturbation and the negative SW forcing of the SRM intervention. However, there is a net forcing of the surface for this intervention, and equivalently, a change to the bulk radiative flux divergence of the troposphere. The perturbation to the bulk tropospheric radiative heating is positive (i.e., an anomalous heating) with magnitude +2.72 W/m^2.

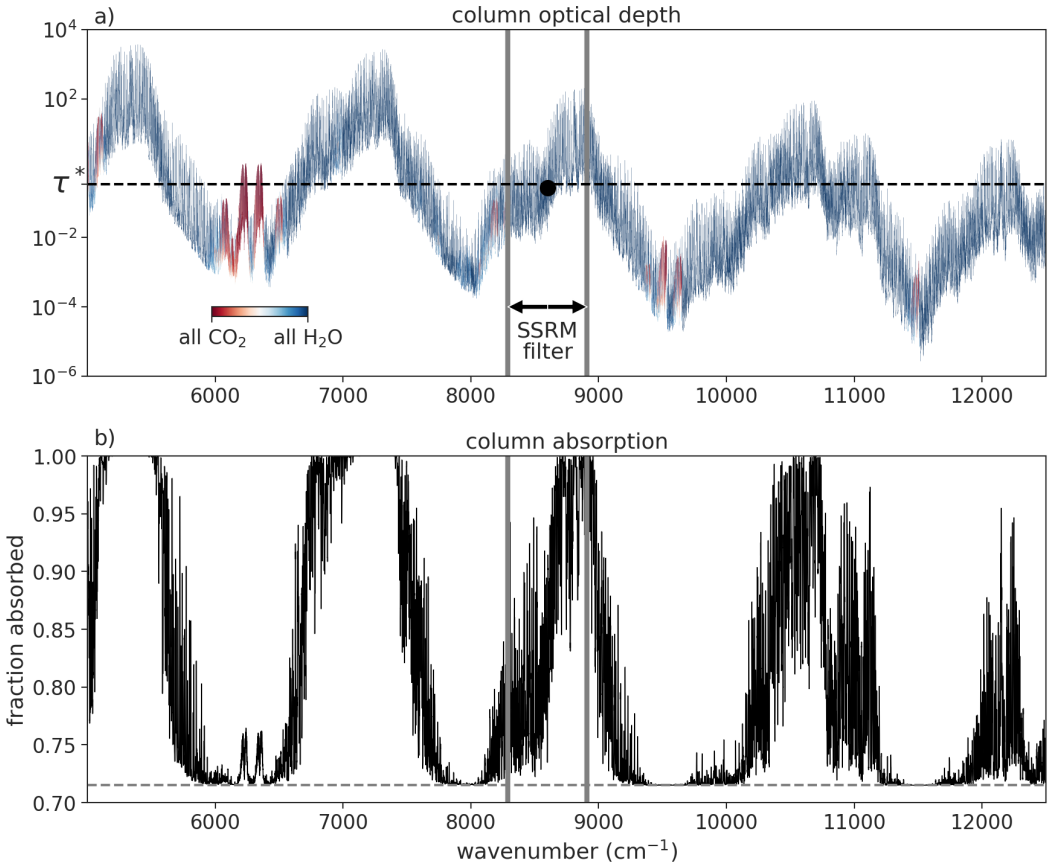

Figure 3. (a) Spectrally-resolved column optical depth from the CTRL experiment in the near-infrared. The data is color-coded according to the fraction of the surface optical depth contributed by H_2O versus CO_2. The optimal optical depth for offsetting CO_2 forcing at the tropopause and surface simultaneously, τ^*, is indicated by the horizontal dashed line. The spectral SRM filter spans the wavenumber range 8290–8910 cm^{-1} and is indicated by the gray bars. The (geometric) mean optical depth within the filtered band is indicated by the filled circle. (b) Spectrally-resolved column absorption from CTRL in the near-infrared. The surface co-albedo (i.e., 1 minus the surface albedo) is plotted as the horizontal dashed line, and sets the minimum column absorption (i.e., for a transparent atmosphere).

The LW effect of the CO_2 perturbation on the radiative cooling of the atmosphere is slightly larger than this, but is partially offset by a small anomalous shortwave cooling due to the USRM intervention.

The goal of spectrally-tuned solar dimming, on the other hand, is to *completely* offset the direct effect of CO_2 by producing a larger anomalous shortwave cooling of the

troposphere. Here we suggest that this can be accomplished by concentrating the solar dimming in the near-infrared wavelengths (roughly 5000–12500 cm^{-1}), where H_2O has strong absorption bands that are primarily responsible for the shortwave heating of the troposphere. Specifically, to ensure a quantitatively accurate filter, we must choose γ_i to satisfy equations 10–11. By trial and error, we found that setting $\gamma_i = 1$ in the wavenumber range 8290-8910 cm^{-1} accomplishes this goal (Fig. 3). Note that the opacity in this band is attributable almost entirely to H_2O. There are other filters that also satisfy equations 10–11, but we will take the filter shown in Figure 3 as our example of spectrally-tuned SRM (SSRM). The third column in Figure 2b shows that this filter, when combined with a quadrupling of CO_2, produces no net forcing at the tropopause *or* surface, and therefore no anomalous bulk radiative heating of the troposphere. The filter works because it contains the correct balance of optically-thin and optically-thick wavelengths: although the optical depths within this band span roughly 4 orders of magnitude, the (geometric) mean optical depth within the filtered band is very close to the optimal optical depth $\tau^* = 0.34$ calculated by setting the right-hand side of equation (8) equal to ϵ_{CO_2} and solving for τ_i (Fig. 3a). The most optically-thick wavelengths within the filtered band are almost entirely absorbed within the troposphere, whereas the most optically-thin wavelengths are absorbed only at the surface (Fig. 3b).

Although the SSRM filter nullifies the direct effect of CO_2 on *bulk* tropospheric radiative heating, the vertically-resolved compensation is not exact (Fig. 3a). This slight redistribution of radiative heating rates in the vertical could, in principle, affect atmospheric dynamics.

4 Results

We have seen in Figures 2-3 that it is possible to design a spectrally-tuned SRM intervention that offsets the radiative forcing from CO_2 at the tropopause and at the surface simultaneously. But, does this SSRM approach outperform the USRM approach at the task of maintaining mean temperature and precipitation at their unperturbed values? Figure 4 shows time series of surface temperature and precipitation from the branched RCE experiments. The surface warms rapidly in the $4\times CO_2$ experiment, eventually equilibrating at a surface temperature warmer by $\Delta T_s = 6.89$ K after approximately 3 years of model time. Therefore, the equilibrium climate sensitivity for our model configuration is approximately 3.5 K, squarely within the best-estimate range for ECS (S. Sher-

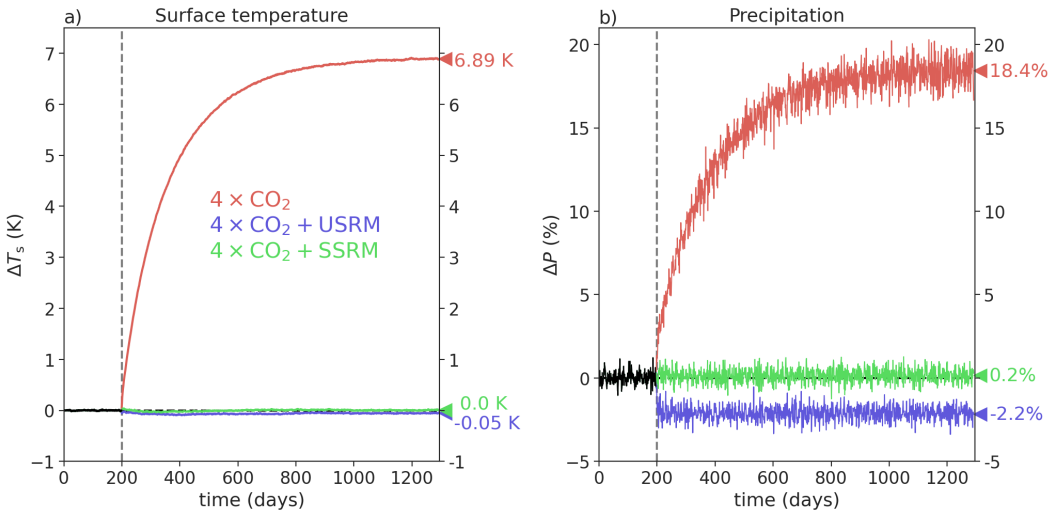

Figure 4. Anomaly timeseries of (a) slab-ocean temperature T_s and (b) precipitation rate P from the DAM experiments. The three experiments with quadrupled CO_2 are branched from CTRL at day 200 and run for 3 additional years of model time. The precipitation timeseries is plotted as a moving average with a centered window of 1 week to reduce noise. Quantities averaged over the final 100 days of the simulations are marked on the ordinates at right.

wood et al., 2020). This large warming causes an increase in mean precipitation of 18.4%, or roughly 2.7 %/K, which is the expected effect of a deepening troposphere under warming (Jeevanjee & Romps, 2018).

Both SRM interventions (USRM and SSRM) greatly reduce the magnitude of changes to temperature and precipitation. For surface temperature, the two interventions are roughly equally effective: both limit the magnitude of changes in surface temperature to ≤ 0.05 K, more than two orders of magnitude smaller than the warming caused by quadrupling CO_2 without any form of SRM. For precipitation, however, the effectiveness of the SRM interventions differs greatly: USRM causes a decrease in mean precipitation of -2.2%, whereas SSRM limits the change in precipitation to less than +0.2%. Therefore, the SSRM intervention is indeed a more complete radiative antidote to CO_2 forcing than the USRM intervention, because it nullifies both the greenhouse effect of CO_2 on surface temperature and the direct effect of CO_2 on precipitation. These results are summarized in Table 1.

	4×CO_2	4×CO_2+USRM	4×CO_2+SSRM
F_t (W/m^2)	9.71	-0.105	-0.155
F_s (W/m^2)	4.63	-2.82	-0.04
ΔT_s (K)	6.89	-0.055	0.005
ΔP (%)	18.4	-2.16	0.157

Table 1. Radiative forcings at the tropopause (F_t) and surface (F_s), as well as mean changes in surface temperature T_s and precipitation P, from the three DAM experiments with quadrupled CO_2.

5 Discussion

In this study, we have developed the theory of spectrally-tuned SRM interventions. Such interventions have the goal of simultaneously maintaining mean surface temperature and mean precipitation at their unperturbed values even as large quantities of CO_2 are added to the atmosphere. Theoretically, this is made possible by the strong absorption bands of H_2O in the near-infrared: by concentrating solar dimming at these wavelengths, it is possible to produce an anomalous shortwave cooling of the troposphere that offsets the longwave heating of additional CO_2. Equivalently, a successful spectrally-tuned solar dimming preserves the energy budget of the tropopause and the surface (equations 10–11), whereas spectrally-flat solar dimming can preserve the energy budget at the tropopause but leaves the surface energy budget perturbed.

As a proof-of-principle, we have demonstrated the success of spectrally-tuned SRM in idealized cloud-resolving model experiments. Although we have only investigated SSRM in a configuration that entirely offsets CO_2 forcing at the tropopause (in accordance with the GeoMIP G1 protocol; Kravitz et al., 2011), our results can be generalized to help understand the effects of SRM interventions that offset only a fraction of CO_2 forcing. Suppose that an SRM intervention is designed such that $F_t^{\mathrm{SRM}} = -\beta F_t^{\mathrm{CO_2}}$, for $0 \leq \beta \leq 1$ (i.e., $\beta = 0$ corresponds to no offsetting of CO_2 forcing, while $\beta = 1$ corresponds to complete offsetting). Combining equations (1–5), we obtain the following expression for the change in precipitation, which generalizes equation (6):

$$\Delta P = -\alpha_P F_{\mathrm{t}}^{\mathrm{CO_2}} \Big[\underbrace{(1-\beta) + \beta\epsilon_{\mathrm{SRM}} - \epsilon_{\mathrm{CO_2}}}_{\text{direct effect}} + \underbrace{\frac{\partial Q}{\partial T_{\mathrm{s}}} \alpha_T (1-\beta)}_{\text{warming effect}} \Big], \quad (12)$$

where we have indentified with underbraces the two sources of changes in precipitation: 1) the direct effect from the combination of a CO_2 perturbation and an SRM intervention, and 2) the effect of warming on precipitation. By putting in representative numbers, we can use equation (12) to make several useful observations. Consider first CO_2 forcing alone ($\beta = 0$). Taking $\epsilon_{\mathrm{CO_2}} = 0.5$, $\frac{\partial Q}{\partial T_{\mathrm{s}}} = -3$ W/m^2/K (Jeevanjee & Romps, 2018), and $\alpha_T = 0.7$ K/W/m^2 (as inferred from our $4\times CO_2$ experiment, in which a $\simeq$ 10 W/m^2 tropopause forcing causes a $\simeq 7$ K warming), equation (12) suggests that the direct effect of CO_2 on precipitation is smaller than the warming effect by a factor of about 1/4, close to the estimate of Romps (2020). This implies that, if the goal is to minimize disruption to the hydrological cycle, minimizing changes in surface temperature via the tropopause energy budget is the most powerful lever. It is only when $\beta \simeq 1$, as in our experiments and the G1 experiment protocol, that the warming effect is suppressed enough to allow the direct effect to dominate changes in precipitation; in this limit, equation (12) shows that the direct effect is controlled by the difference $\epsilon_{\mathrm{SRM}} - \epsilon_{\mathrm{CO_2}}$, as previously discussed in section 2 (c.f. equation 6, Fig. 1). In this limit, if the goal is to minimize the perturbation to the mean precipitation rate, the spectral properties of the SRM intervention should be tuned so that $\epsilon_{\mathrm{SRM}} = \epsilon_{\mathrm{CO_2}}$. In general, the optimal value of ϵ_{SRM} will depend on the strength of the SRM intervention as well as the objective function.

Given the success of spectral SRM in our idealized model, it is natural to wonder how spectral SRM might be realized in the real world. At present, there is no off-the-shelf commercial technology that could be used to implement spectral SRM without prohibitive costs and environmental impacts. Yet, SRM would likely be implemented over a time scale of a century or more, so there is time for technological innovation, and already there are signs that "designer materials" with tuneable extinction coefficients at near-infrared wavelengths may be within reach. Metallic nanoparticles that exhibit optical plasmonic resonance (Khlebtsov & Dykman, 2010) can exhibit narrow-band scattering or absorption in the optical and near-infrared, with resonant spectral widths of order 1000 wavenumbers (Berkovitch et al., 2010) — consistent with the size of filter we analyze in this work. Diffractive structures and resonant scatterers for SRM were proposed over two decades ago (Teller et al., 1997); similarly, self-levitating atmospheric scat-

terers for SRM were proposed a decade ago (D. W. Keith, 2010), and are now being physically demonstrated in the lab (Cortes et al., 2020). A small but growing body of literature has explored space-based SRM since 1989, and several of these proposals exploit diffractive screens (Angel, 2006). All of these methods could serve as the basis for spectrally-tunable SRM interventions.

Even if it turns out that spectrally-tuned SRM technologies will never be practical or cheap enough for use, our results remain relevant to more mainstream approaches to SRM (e.g., with stratospheric sulfate aerosols), for the simple reason that any real-world implementation of SRM will not be spectrally uniform. We have shown how to map the spectral characteristics of candidate SRM technologies onto their expected impacts on mean precipitation, thereby providing a new metric for evaluating such technologies. Indeed, prior work has shown that different SRM technologies have different effects on precipitation rates (Niemeier et al., 2013). Our results indicate that one potential source of such differences is the different spectral characteristics of the proposed technologies; future work could assess this possibility with the aid of equations (10–11), which provide a quick method of parsing the "design space" of SRM technologies without resorting to computationally-expensive simulations with global climate models.

Overall, although our results regarding the potential of spectral SRM are promising, many questions remain. It is important to realize that designing a radiative antidote to CO_2 is substantially easier for atmospheres that are statistically homogeneous in the horizontal (e.g., our RCE simulations). On the real Earth, spatial heterogeneity in surface temperature, water vapor content, and albedo would cause the ideal spectral SRM intervention itself to be spatially heterogeneous. Another weakness of the theory of spectral SRM developed here is that the surface Bowen ratio is unconstrained, which means that the precipitation rate could change even when the radiative energy budget of the troposphere is unperturbed. This effect could be especially important in models with heterogeneous surface conditions. Global models are the only way to assess changes to regional precipitation, which are more relevant to society than the global-mean change. For these reasons and more, future work should test the effectiveness of spectral SRM in comprehensive global models. It seems possible that SRM interventions that are less disruptive of the tropospheric energy balance will be less disruptive of the climate on a regional scale, but further work is needed to verify this hypothesis.

Acknowledgments

Simulation data and Python source code for reproducing the figures in this manuscript is available at https://doi.org/10.5281/zenodo.4035201.

References

Allen, M. R., & Ingram, W. J. (2002, sep). Constraints on future changes in climate and the hydrologic cycle. *Nature*, *419*(6903), 224–32. doi: 10.1038/nature01092

Andrews, T., Forster, P. M., Boucher, O., Bellouin, N., & Jones, A. (2010). Precipitation, radiative forcing and global temperature change. *Geophysical Research Letters*, *37*(14). doi: 10.1029/2010GL043991

Angel, R. (2006). Feasibility of cooling the Earth with a cloud of small spacecraft near the inner Langrange point (L1). *Proceedings of the National Academy of Sciences of the United States of America*, *103*(46), 17184–17189. doi: 10.1073/pnas.0608163103

Bala, G., Duffy, P. B., & Taylor, K. E. (2008). Impact of geoengineering schemes on the global hydrological cycle. *Proceedings of the National Academy of Sciences*, *2008*.

Berkovitch, N., Ginzburg, P., & Orenstein, M. (2010). Concave plasmonic particles: Broad-band geometrical tunability in the near-infrared. *Nano Letters*, *10*(4), 1405–1408. doi: 10.1021/nl100222k

Clough, S. A., Iacono, M. J., & Moncet, J.-l. (1992). Line-by-line calculations of atmospheric fluxes and cooling rates: Application to water vapor. *Journal of Geophysical Research*, *97*(D14), 15761.

Clough, S. A., Shephard, M. W., Mlawer, E. J., Delamere, J. S., Iacono, M. J., Cady-Pereira, K., ... Brown, P. D. (2005). Atmospheric radiative transfer modeling: A summary of the AER codes. *Journal of Quantitative Spectroscopy and Radiative Transfer*, *91*(2), 233–244. doi: 10.1016/j.jqsrt.2004.05.058

Cortes, J., Stanczak, C., Azadi, M., Narula, M., Nicaise, S. M., Hu, H., & Bargatin, I. (2020). Photophoretic Levitation of Macroscopic Nanocardboard Plates. *Advanced Materials*, *32*(16), 1–7. doi: 10.1002/adma.201906878

Cronin, T. W. (2014). On the Choice of Average Solar Zenith Angle. *Journal of the Atmospheric Sciences*, *71*(8), 2994–3003. doi: 10.1175/JAS-D-13-0392.1

Dinh, T., & Fueglistaler, S. (2017). Mechanism of Fast Atmospheric Energetic Equi-

libration Following Radiative Forcing by CO2. *Journal of Advances in Modeling Earth Systems*, *9*(7), 2468–2482. doi: 10.1002/2017MS001116

Gordon, I. E., Rothman, L. S., Hill, C., Kochanov, R. V., Tan, Y., Bernath, P. F., ... Zak, E. J. (2017). The HITRAN2016 molecular spectroscopic database. *Journal of Quantitative Spectroscopy & Radiative Transfer*, *203*, 3–69. doi: 10.1016/j.jqsrt.2017.06.038

Govindasamy, B., & Caldeira, K. (2000). Geoengineering Earth's radiation balance to mitigate CO2-induced climate change. *Geophysical Research Letters*, *27*(14), 2141–2144.

Haigh, J. D., Winning, A. R., Toumi, R., & Harder, J. W. (2010). An influence of solar spectral variations on radiative forcing of climate. *Nature*, *467*(7316), 696–699. Retrieved from `http://dx.doi.org/10.1038/nature09426` doi: 10.1038/nature09426

Huang, Y., Xia, Y., & Tan, X. (2017). On the pattern of CO ₂radiative forcing and poleward energy transport. *Journal of Geophysical Research: Atmospheres*, 578–593.

Iacono, M. J., Delamere, J. S., Mlawer, E. J., Shephard, M. W., Clough, S. A., & Collins, W. D. (2008). Radiative forcing by long-lived greenhouse gases: Calculations with the AER radiative transfer models. *Journal of Geophysical Research Atmospheres*, *113*(13), 2–9. doi: 10.1029/2008JD009944

Irvine, P., Emanuel, K., He, J., Horowitz, L. W., Vecchi, G., & Keith, D. (2019). Halving warming with idealized solar geoengineering moderates key climate hazards. *Nature Climate Change*, *9*(4), 295–299. doi: 10.1038/s41558-019-0398-8

Irvine, P. J., Kravitz, B., Lawrence, M. G., & Muri, H. (2016). An overview of the Earth system science of solar geoengineering. *Wiley Interdisciplinary Reviews: Climate Change*, *7*(6), 815–833. doi: 10.1002/wcc.423

Jeevanjee, N., & Romps, D. M. (2018). Mean precipitation change from a deepening troposphere. *Proceedings of the National Academy of Sciences*, *115*(45), 11465–11470.

Keith, D. (2013). A case for climate engineering. *A Case for Climate Engineering*, 1–199. doi: 10.7551/mitpress/9920.001.0001

Keith, D. W. (2010). Photophoretic levitation of engineered aerosols for geoengineering. *Proceedings of the National Academy of Sciences of the United States of*

America, *107*(38), 16428–16431. doi: 10.1073/pnas.1009519107

Khlebtsov, N. G., & Dykman, L. A. (2010). Optical properties and biomedical applications of plasmonic nanoparticles. *Journal of Quantitative Spectroscopy and Radiative Transfer*, *111*(1), 1–35. Retrieved from `http://dx.doi.org/10.1016/j.jqsrt.2009.07.012` doi: 10.1016/j.jqsrt.2009.07.012

Kleidon, A., Kravitz, B., & Renner, M. (2015). The hydrological sensitivity to global warming and solar geoengineering derived from thermodynamic constraints. *Geophysical Research Letters*, *42*(1), 138–144. doi: 10.1002/2014GL062589

Kravitz, B., Caldeira, K., Boucher, O., Robock, A., Rasch, P. J., Alterskjær, K., ... Yoon, J.-h. (2013). Climate model response from the Geoengineering Model Intercomparison Project (GeoMIP). *Journal of Geophysical Research: Atmospheres*, *118*, 8320–8332. doi: 10.1002/jgrd.50646

Kravitz, B., Rasch, P. J., Forster, P. M., Andrews, T., Cole, J. N., Irvine, P. J., ... Yoon, J. H. (2013). An energetic perspective on hydrological cycle changes in the Geoengineering Model Intercomparison Project. *Journal of Geophysical Research Atmospheres*, *118*(23), 13,087–13,102. doi: 10.1002/2013JD020502

Kravitz, B., Robock, A., Boucher, O., Schmidt, H., Taylor, K. E., Stenchikov, G., & Schulz, M. (2011). The Geoengineering Model Intercomparison Project (GeoMIP). *Atmospheric Science Letters*, *12*(2), 162–167. doi: 10.1002/asl.316

Krueger, S. K., Fu, Q., Liou, K. N., & Chin, H.-N. S. (1995, mar). Improvements of an Ice-Phase Microphysics Parameterization for Use in Numerical Simulations of Tropical Convection. *Journal of Applied Meteorology*, *34*, 281–287.

Lambert, F. H., & Faull, N. E. (2007). Tropospheric adjustment: The response of two general circulation models to a change in insolation. *Geophysical Research Letters*, *34*(3), 2–6. doi: 10.1029/2006GL028124

Lin, Y.-L., Farley, R. D., & Orville, H. D. (1983). *Bulk Parameterization of the Snow Field in a Cloud Model* (Vol. 22) (No. 6).

Lord, S. J., Willoughby, H. E., & Piotrowicz, J. M. (1984, oct). Role of a Parameterized Ice-Phase Microphysics in an Axisymmetric, Nonhydrostatic Tropical Cyclone Model. *Journal of the Atmospheric Sciences*, *41*(19), 2836–2848.

Lutsko, N. J., Seeley, J. T., & Keith, D. W. (2020). Estimating Impacts and Trade-offs in Solar Geoengineering Scenarios With a Moist Energy Balance Model. *Geophysical Research Letters*, *47*(9), 1–12. doi: 10.1029/2020GL087290

Niemeier, U., Schmidt, H., Alterskjær, K., & Kristjánsson, J. E. (2013). Solar irradiance reduction via climate engineering: Impact of different techniques on the energy balance and the hydrological cycle. *Journal of Geophysical Research Atmospheres*, *118*(21), 11,905–11,917. doi: 10.1002/2013JD020445

O'Gorman, P. a., Allan, R. P., Byrne, M. P., & Previdi, M. (2011, nov). Energetic Constraints on Precipitation Under Climate Change. *Surveys in Geophysics*, *33*(3-4), 585–608. doi: 10.1007/s10712-011-9159-6

Pendergrass, A. G., & Hartmann, D. L. (2014, jan). The Atmospheric Energy Constraint on Global-Mean Precipitation Change. *Journal of Climate*, *27*(2), 757–768. doi: 10.1175/JCLI-D-13-00163.1

Preston, C. J. (2013). Ethics and geoengineering: Reviewing the moral issues raised by solar radiation management and carbon dioxide removal. *Wiley Interdisciplinary Reviews: Climate Change*, *4*(1), 23–37. doi: 10.1002/wcc.198

Romps, D. M. (2008). The Dry-Entropy Budget of a Moist Atmosphere. *Journal of the Atmospheric Sciences*, *65*(12), 3779–3799.

Romps, D. M. (2011). Response of Tropical Precipitation to Global Warming. *Journal of the Atmospheric Sciences*, *68*(1), 123–138.

Romps, D. M. (2014, oct). An Analytical Model for Tropical Relative Humidity. *Journal of Climate*, *27*(19), 7432–7449.

Romps, D. M. (2020). Climate Sensitivity and the Direct Effect of Carbon Dioxide in a Limited-Area Cloud-Resolving Model. *Journal of Climate*, *33*(9), 3413–3429. doi: 10.1175/jcli-d-19-0682.1

Romps, D. M., & Kuang, Z. (2010). Do Undiluted Convective Plumes Exist in the Upper Tropical Troposphere? *Journal of the Atmospheric Sciences*, *67*, 468–484.

Seeley, J. T., Jeevanjee, N., Langhans, W., & Romps, D. M. (2019). Formation of Tropical Anvil Clouds by Slow Evaporation. *Geophysical Research Letters*, *46*(1), 492–501.

Seeley, J. T., Jeevanjee, N., & Romps, D. M. (2019). FAT or FiTT: Are anvil clouds or the tropopause temperature-invariant? *Geophysical Research Letters*, *46*(3), 1842–1850.

Seeley, J. T., & Romps, D. M. (2015). Why does tropical convective available potential energy (CAPE) increase with warming? *Geophysical Research Letters*, *42*(23), 10429–10437.

Seeley, J. T., & Romps, D. M. (2016). Tropical cloud buoyancy is the same in a world with or without ice. *Geophysical Research Letters*, n/a—-n/a.

Sherwood, S., Webb, M. J., Annan, J. D., Armour, K. C., Forster, P. M., Hargreaves, J. C., ... Zelinka, M. D. (2020). An assessment of Earth's climate sensitivity using multiple lines of evidence. *Reviews of Geophysics*, 1–166.

Sherwood, S. C., Bony, S., Boucher, O., Bretherton, C., Forster, P. M., Gregory, J. M., & Stevens, B. (2015). ADJUSTMENTS IN THE FORCING – FEEDBACK FRAMEWORK FOR UNDERSTANDING CLIMATE. *Bulletin of the American Meteorological Society*(February), 217–228. doi: 10.1175/BAMS-D-13-00167.1

Simpson, I. R., Tilmes, S., Richter, J. H., Kravitz, B., MacMartin, D. G., Mills, M. J., ... Pendergrass, A. G. (2019). The Regional Hydroclimate Response to Stratospheric Sulfate Geoengineering and the Role of Stratospheric Heating. *Journal of Geophysical Research: Atmospheres*, *124*(23), 12587–12616. doi: 10.1029/2019JD031093

Smith, C. J., Kramer, R. J., Myhre, G., Forster, P. M., Soden, B. J., Andrews, T., ... Watson-Parris, D. (2018). Understanding Rapid Adjustments to Diverse Forcing Agents. *Geophysical Research Letters*, *45*(21), 12,12–23,31.

Smyth, J. E., Russotto, R. D., & Storelvmo, T. (2017). Thermodynamic and dynamic responses of the hydrological cycle to solar dimming. *Atmospheric Chemistry and Physics*, *17*(10), 6439–6453. doi: 10.5194/acp-17-6439-2017

Teller, E., Wood, L., & Hyde, R. (1997). *Global Warming and Ice Ages: I. Prospects for Physics-Based Modulation of Global Change.*

Tilmes, S., Fasullo, J., Lamarque, J.-f., Marsh, D. R., Mills, M., Alterskjær, K., ... Niemeier, U. (2013). The hydrological impact of geoengineering in the Geoengineering Model Intercomparison Project (GeoMIP). *Journal of Geophysical Research: Atmospheres*, *118*, 36–58. doi: 10.1002/jgrd.50868

Wordsworth, R., Kalugina, Y., Lokshtanov, S., Vigasin, A., Ehlmann, B., Head, J., ... Wang, H. (2017). Transient reducing greenhouse warming on early Mars. *Geophysical Research Letters*, 1–7. doi: 10.1002/2016GL071766